

# Friction Boosted by Equilibrium Misalignment of Incommensurate Two-Dimensional Colloid Monolayers

Davide Mandelli<sup>1</sup>, Andrea Vanossi<sup>2,1</sup>, Nicola Manini<sup>3,1,2</sup>, Erio Tosatti<sup>1,2,4</sup>

<sup>1</sup> *International School for Advanced Studies (SISSA), Via Bonomea 265, 34136 Trieste, Italy*

<sup>2</sup> *CNR-IOM Democritos National Simulation Center, Via Bonomea 265, 34136 Trieste, Italy*

<sup>3</sup> *Dipartimento di Fisica, Università degli Studi di Milano, Via Celoria 16, 20133 Milano, Italy*

<sup>4</sup> *International Centre for Theoretical Physics (ICTP), Strada Costiera 11, 34014 Trieste, Italy*

(Dated: March 19, 2015)

Colloidal 2D monolayers sliding in an optical lattice are of recent importance as a frictional system. In the general case when the monolayer and optical lattices are incommensurate, we predict two important novelties, one in the static equilibrium structure, the other in the frictional behavior under sliding. Structurally, realistic simulations show that the colloid layer should possess in full equilibrium a small misalignment rotation angle relative to the optical lattice, an effect so far unnoticed but visible in some published experimental moiré patterns. Under sliding, this misalignment has the effect of boosting the colloid monolayer friction by a considerable factor over the hypothetical aligned case discussed so far. A frictional increase of similar origin must generally affect other incommensurate adsorbed monolayers and contacts, to be sought out case by case.

PACS numbers: 68.35.As,68.35.Gy,83.10.Rs,82.70.Dd

The mutual sliding of crystalline lattices offers, despite its apparently academic nature, one of the basic platforms to understand the nanoscale and mesoscale frictional and adhesion phenomena [1]. In one of the freshest developments, Bohlein and collaborators [2] showed that the sliding of a 2D crystalline monolayer of colloidal particles in an optical lattice provides unexpected information on elementary tribological processes in crystalline sliding systems with ideally controlled commensurabilities. Given the scarcity of reliable and controllable frictional systems, it is hard to overestimate the importance of such model systems with full external control over all parameters including periodicity, coupling strengths, and applied forces. For this reason 2D monolayers in periodic lattices require a close theoretical study. In this letter we describe two main surprises, one structural and one frictional, which emerge from realistic molecular dynamics simulations. We show first of all that incommensurate colloid islands naturally develop in full equilibrium a small misalignment angle relative to the substrate. Second, sliding simulations demonstrate that the misaligned angular orientation increases significantly the dynamic friction with respect to the (hypothetical and unstable) aligned case. While both are important for colloidal monolayers, their potential impact extends in principle beyond the specific case, to a wider variety of systems where mutually incommensurate 2D lattices are brought in static and then in sliding contact.

In colloid monolayers, the 2D density may vary from “underdense” ( $\rho < 1$ , where  $\rho = a_l/a_c$ , with  $a_l$  the spacing of the optical lattice,  $a_c$  that of the colloid lattice, both triangular) to perfectly commensurate ( $\rho = 1$ , one particle per potential well), to “overdense” ( $\rho > 1$ ), each with its specific sliding behavior. Both experiments [2] and theory [3, 4] indicated that commensurate ( $\rho = 1$ )

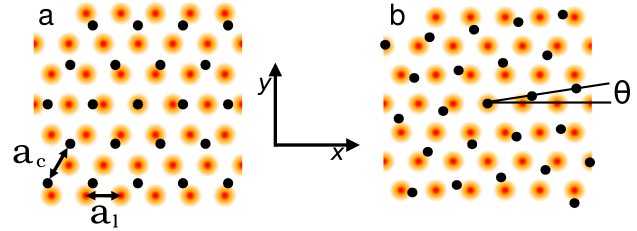


FIG. 1. (Color online) (a) Schematic of a 2D colloidal lattice (black dots) aligned with an incommensurate triangular periodic potential mimicking the optical lattice (blurred spots represent potential minima). (b) A misaligned configuration rotated by an angle  $\theta$ .

friction is large, dropping to much lower values for  $\rho \neq 1$ , where optical and colloid lattice are incommensurate. This drop reflects the great mobility of the pre-existing misfit dislocations, also called kinks or “solitons”. In these studies the two lattices, colloid and optical, were silently assumed to be geometrically aligned, prior to and during sliding. That assumption however is dangerous. A long-known theoretical result suggests [5], for example, that a harmonic monolayer subject to an incommensurate periodic potential of weak amplitude  $U_0$  may partly convert the misfit compressional stress to shear stress by an equilibrium geometric misalignment of the monolayer (see Fig. 1) through a small rotation angle

$$\theta_{\text{NM}} = \arccos \left( \frac{1 + \rho^2(1 + 2\delta)}{\rho[2 + \delta(1 + \rho^2)]} \right), \quad (1)$$

whose energy-lowering effect originates from a better interdigitation of the two lattices. Independent of  $U_0$ , the rotation angle is nonzero in this approximation provided the transverse 2D sound velocity  $c_T$  is sufficiently smaller than the longitudinal  $c_L$ , precisely if  $\delta = (c_L/c_T)^2 - 1 >$

$\rho^{-1}$ . While this kind of rotated epitaxy has been addressed experimentally [6, 7] and theoretically [8] for adsorbed rare-gas monolayers, its possible presence in colloidal monolayers was so far unsuspected. More importantly in the context of sliding friction, the tribological impact of an *equilibrium* geometrical misalignment is unexplored in any incommensurate system. The externally forced rotation turning a *commensurate* layer into incommensurate is well known to reduce friction, as exemplified by the sliding of graphene flakes on graphite [10, 11]. Different as these two cases are, a possible expectation might be that the equilibrium geometry, alignment of commensurate layers, or misalignment of incommensurate layers, should always exhibit a higher friction relative to forcedly rotated ones, since the optimal  $T = 0$  geometry must in every case corresponds to a closer interdigitation of the two lattices.

First, let us consider structural alignment. Using the same methods as in Ref. 3, we model the colloidal system in an optical lattice as a 2D monolayer of  $N_p$  point-like classical particles, mutually repelling through a screened Coulomb potential  $U_{pp}(r_{ij})$  while immersed in a static 2D triangular lattice potential  $W(\mathbf{r}_i) = U_0 w(\mathbf{r}_i)$  where  $w(\mathbf{r})$  is a dimensionless periodic function of spacing  $a_l$  (as specified in Supplemental Material (SM)), and  $U_0$  is the amplitude (“corrugation”) parameter. The Hamiltonian is thus

$$H = \sum_{i=1}^{N_p} \left[ U_0 w(\mathbf{r}_i) + \frac{1}{2} \sum_{j \neq i} U_{pp}(r_{ij}) \right]. \quad (2)$$

The particles are confined to the  $(x, y)$  plane, and subjected to either planar periodic boundary conditions (PBC) in a given area  $A$ , or alternatively to an additional Gaussian confining potential  $G(r) = -A_G \exp(-r^2/\sigma_G^2)$ , in which case they form an island with open boundary conditions (OBC). Temperature is generally set to zero, because the results are clearer and require less statistics in this limit. Finite temperature results are otherwise not essentially different, as shown along with details of optimization protocols in Supplemental Material (SM). Within the confinement region the 2D particles crystallize in a triangular lattice of mean spacing  $a_c$ , with modulations induced by the periodic potential (in the OBC case there is also a confinement-induced variation between a dense center and a sparser periphery). Here and in the rest we shall focus for specificity on the underdense incommensurate case  $\rho = 3/(1 + \sqrt{5}) \simeq 0.927$ ; the physics with different values of  $\rho \neq 1$  including  $\rho > 1$  is qualitatively similar, as briefly discussed in SM.

We determined, by means of careful energy minimization, the optimal  $T = 0$  2D geometry of all  $N_p$  particles for increasing corrugation strength; shown here are the results for  $U_0 = 0.1 - 0.6$ , where the effects are particularly clear. The final, optimal geometry of the 2D colloid lattice initially aligned at  $\theta = 0^\circ$  with the optical lat-

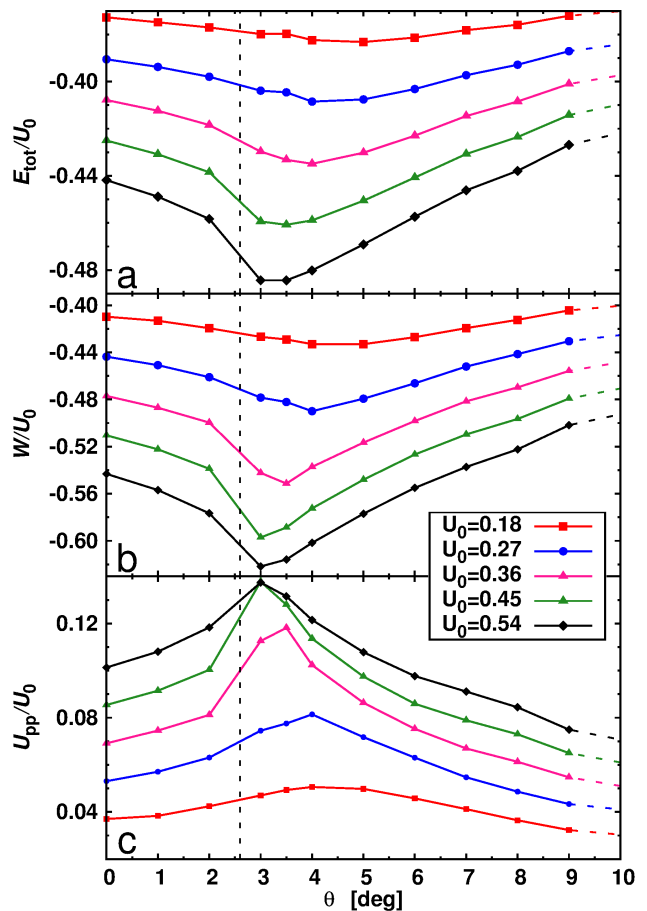


FIG. 2. (Color online) Relative static energy of structure-optimized colloid islands (OBC) as a function of the trial rotation angle  $\theta$ . (a) Total energy per particle  $E_{\text{tot}}$ . (b) Periodic-potential (corrugation) contribution  $W$  to  $E_{\text{tot}}$ . (c) Interparticle interaction contribution  $U_{pp}$  to  $E_{\text{tot}}$ . Curves correspond to increasing corrugation amplitude  $U_0 = 0.18 - 0.54$ . Energies are measured relative to that of the colloidal monolayer at rest and at  $U_0 = 0$ . Dashed line: ideal NM angle, Eq. (1),  $\theta_{\text{NM}} \approx 2.6^\circ$ .

tice axes is found to be misaligned, with a small rotation angle  $\theta_{\text{opt}} \simeq 2.3^\circ$  in PBC calculations. This rotation realizes a better interdigitation with the optical lattice, and occurs spontaneously during the simulation at the cost of creating the dislocations required by the PBC constraints (see SM). More detailed energy minimizations were done in OBC, which do not have the same problem. Since the 30,000 particle islands are too large to spontaneously rotate, we carried out simulations starting from a prearranged sequence of misalignment angles. The total energy minimum versus  $\theta$  confirms, as shown by Fig. 2, the structural misalignment angle at equilibrium, with a magnitude in the range  $3^\circ < \theta_{\text{opt}} < 5^\circ$  (depending on the optical lattice strength  $U_0$ ) generally somewhat larger than in PBC, where angular constraints hinder the misalignment.

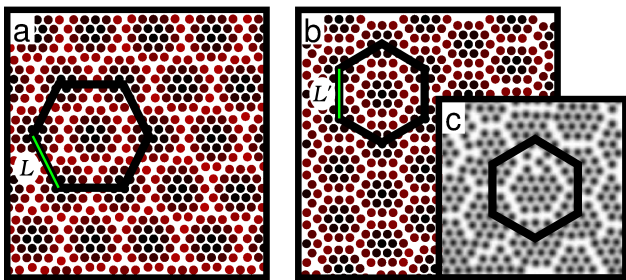


FIG. 3. (Color online) Equilibrium configurations obtained for  $\rho \simeq 0.83$  and  $U_0 = 6.3$ . (a) Unrotated  $\theta = 0^\circ$ ; (b) optimally rotated  $\theta_{\text{opt}} = 7^\circ$ . Dark/light colloids enjoy best/worse  $W$ . Only the central part of the island, optimized in OBC, is shown. (c) Experimental geometry for the same  $\rho$ , adapted from Ref. 12, where both the moiré angles and spacing compare directly with (b) rather than (a).

These structural results compare instructively with those expected from the harmonic model [5]. In our case a 2D phonon calculation for the monolayer yields a sound velocity ratio  $c_L/c_T = 1.806$ , larger than the theoretical threshold value  $(1 + \rho^{-1})^{1/2} \simeq 1.442$ . The corresponding theoretical misalignment  $\theta_{\text{NM}} \simeq 2.6^\circ$  is in qualitative agreement with the more realistic simulation result. Figure 2b,c shows how the two pieces which compose the total energy, namely the periodic lattice energy part  $W = \langle W(\mathbf{r}_i) \rangle$  controlled by the corrugation amplitude  $U_0$  and the interparticle interaction  $U_{\text{pp}} = \langle U_{\text{pp}}(r_{ij}) \rangle$ , behave. Misalignment raises the interparticle energy, but that cost is overcompensated, by a factor 2, by a corrugation energy gain. The incommensurate colloid static equilibrium structure is misaligned because that permits a better interdigitation with the optical lattice.

Even if our predicted misalignments are small, their experimental existence is easily revealed, because the rotation angle  $\theta$  between two lattices is highly amplified by the moiré pattern, which rotates relative to the periodic potential lattice by an angle  $\psi$  satisfying the geometric relation  $\cos \theta = \rho^{-1} \sin^2 \psi + \cos \psi [1 - \rho^{-2} \sin^2 \psi]^{1/2}$  [16]. As the moiré superlattice rotates by  $\psi$ , its spacing  $L$  also decreases [17] from its aligned value of about  $L = a_c \rho / (1 - \rho)$  to its rotated value of  $L' = a_c / \sqrt{1 + \rho^{-2} - 2\rho^{-1} \cos \theta}$ . As an example, Fig. 3 reports the structures of the artificially unrotated and of the optimally rotated ( $\theta_{\text{opt}} = 7^\circ$ ) configurations calculated for  $\rho \simeq 0.83$  and  $U_0 = 6.3$  (parameters believed to be appropriate to experiments in Ref. 12) in comparison with one another and with the corresponding experimental structural moiré. Both the orientation and spacing of Fig. 3c agree with the  $\theta_{\text{opt}} = 7^\circ$  but not with the  $\theta_{\text{opt}} = 0^\circ$  pattern, proving that the misalignment was actually present in that experiment.

The particle static displacements associated with the optical lattice potential are also enlightening. Figure 4 shows the moiré pattern of a small portion of the mono-

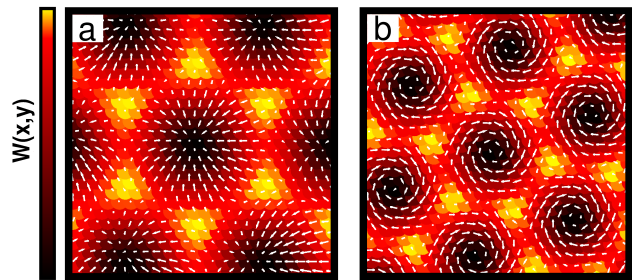


FIG. 4. (Color online) Moiré patterns of the particle monolayer's central region as obtained in OBC for  $\rho = 0.927$ ,  $U_0 = 0.27$ , (a) for  $\theta = 0^\circ$  (moiré angle  $\psi = 0^\circ$ ) and (b) for the optimal  $\theta = 4^\circ$  (moiré angle  $\psi \approx 15^\circ$ ). Each dot indicates a particle in the unrelaxed configuration, colored according to the local corrugation potential  $W(\mathbf{r})$ : dark for potential minima, bright for maxima. White arrows show the displacements of each particle from the ideal triangular lattice to the fully relaxed configuration, magnified 15 times. The compression-dilations at  $\theta = 0^\circ$  are turned into largely shear, vortex-like displacements at  $\theta_{\text{opt}} = 4^\circ$ .

layer island ( $\rho = 0.927$ ,  $U_0 = 0.27$ ) for  $\theta = 0^\circ$  and for  $\theta_{\text{opt}} = 4^\circ$ , corresponding to a moiré angle  $\psi \approx 15^\circ$ . Particle displacements, designated by arrows, change from radial longitudinal compression-dilations to mixed shear-longitudinal, vortex-like displacements upon optimal misalignment. A large 2D bulk modulus and a weak shear rigidity of the crystalline monolayer are crucial factors increasing the extent of the shear distortions, therefore enhancing the lattice misalignment.

We come to our second point, i.e., the forced sliding of the particle monolayer over the periodic corrugation and the associated frictional losses. The shear distortions and the corresponding increased interdigitation at the optimal misalignment angle  $\theta_{\text{opt}}$  are expected to affect the sliding of the particle lattice over the periodic potential. Sliding is realized by a flow of the soliton superstructure, accompanied by dissipation as part of the work goes into soliton-related time-dependent distortions of the 2D lattice. That work will change once the nature (longitudinal to shear), orientation ( $0^\circ$  to  $\psi$ ), periodicity ( $L$  to  $L'$ ) change with  $\theta$  ( $0^\circ$  to  $\theta_{\text{opt}}$ ). We determine the magnitude of the expected friction change by simulating the overdamped sliding dynamics of the OBC island over a range of  $\theta$  values, so as to assess the frictional effect of misalignment near its optimal value. We applied an external driving force  $F_d$  acting on each particle, slowly varying to-and-fro as a function of time, mimicking the experimental drag force  $\eta v_d$  induced by a fluid of viscosity  $\eta$  and slowly back and forth time-dependent speed  $v_d$  [2] (details in SM). Despite a nonzero torque, generally present for all preset angles that differ from  $\theta_{\text{opt}}$  (and from zero) the misalignment angle did not have the time to change appreciably in the course of the simulation. Under sliding, the frictional power dissipated per

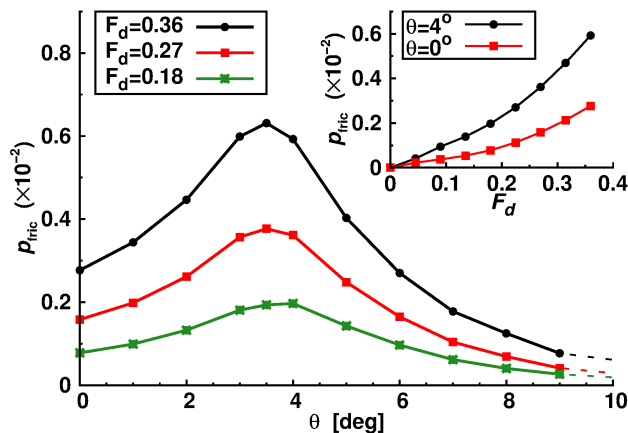


FIG. 5. (Color online) Dissipated friction power  $p_{\text{fric}}$  as a function of the trial misalignment angle  $\theta$  ( $U_0 = 0.27$ ). Three curves are reported corresponding to increasing values of the driving force  $F_d = 0.18, 0.27, 0.36$ . The inset shows  $p_{\text{fric}}$  as a function of  $F_d$  for two values of  $\theta$ .

particle was calculated as [3]

$$p_{\text{fric}} = \mathbf{F}_{\mathbf{d}} \cdot \langle \mathbf{v}_{\text{cm}} \rangle - \eta |\langle \mathbf{v}_{\text{cm}} \rangle|^2 = (\eta/N_p) \sum_i \langle |\mathbf{v}_i - \mathbf{v}_{\text{cm}}|^2 \rangle \quad (3)$$

where  $\mathbf{v}_{\text{cm}}$  is the center-of-mass velocity,  $\mathbf{v}_i$  is the velocity of particle  $i$ , and brackets denote steady-state averages. Due to the confining envelope potential, the lattice spacing  $a_c$ , close to constant in the central part, increases toward the periphery, where colloids also tend to be pinned by the corrugation. To address properties of mobile colloids at a well-defined density, trajectories were analyzed, as also done in experiments, considering only particles belonging to the central portion of the island, in our case a square of size  $80 \times 80 a_c^2$ . The duration of the sliding simulations was fixed by requiring a total center of mass displacement not smaller than  $\Delta x_{\text{cm}} \approx 2 - 3 a_c$ .

Figure 5, our main dynamical result, shows that friction is increased by a very substantial factor by misalignment relative to alignment, reaching a maximum of about two at the optimal angle  $\theta_{\text{opt}}$ , subsequently dropping for larger angles where the energy gain and static distortion magnitude also drop. The physical reason for the frictional peak at  $\theta_{\text{opt}}$  can be further appreciated by looking at the particles' steady state velocity distribution  $P_v$  and at the corresponding static interparticle spacing distribution (at zero velocity)  $P_r$ , both shown in Fig. 6 for increasing  $\theta$ . The important points here are that small interparticle distances are energetically costly, and that a large spread of velocities relative to the center-of-mass denotes larger frictional dissipation, according to the RHS of Eq. (3). At perfect alignment, short distances (colored column) are very frequent, which is energetically costly. At the same time the spread of velocities is moderate and so is friction. In the optimally misaligned case  $\theta_{\text{opt}}$  instead, the shortest distance becomes less frequent,

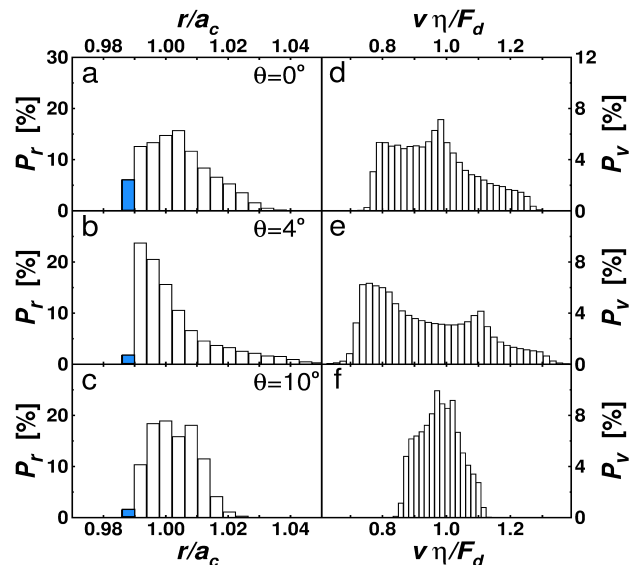


FIG. 6. (Color online) (a-c) The distribution  $P_r$  of nearest-neighbor distances in the static relaxed configurations ( $F_d = 0$ ,  $U_0 = 0.27$ ) at rotation angles  $\theta = 0^\circ$ ,  $\theta = \theta_{\text{opt}} = 4^\circ$ , and  $\theta = 10^\circ$ . (d-f) Corresponding velocity distribution  $P_v$  of particles sliding under an external force  $F_d = 0.36$ .

thus reducing energy as we already know. At the same time however  $P_v$  develops longer tails at lower and higher particle velocities, both of which increase friction. At  $\theta > \theta_{\text{opt}}$  finally the velocity spread drops and so does friction, the monolayer sliding less and less affected by corrugation.

In conclusion, colloid monolayers in an incommensurate optical lattice develop, in full equilibrium and with realistic parameters, a small-angle structural misalignment, quite evident in moiré patterns such as those of Fig. 3. Upon forced sliding, this misalignment can considerably increase the sliding friction, directly extractable from the colloid drift velocity in experiment, using Eq. (3), over the hypothetical aligned geometry.

The present results and understanding naturally extrapolate to the sliding of misaligned incommensurate lattices in contact such as, for example, physisorbed rare-gas or molecular submonolayer islands [6–8]. An interesting side aspect is in this case that misalignment transforms the orientation angle of a physisorbed island, generally assumed to be fixed, into a continuous and possibly dynamical variable. The inertial sliding friction of such islands determines the inverse slip time in quartz crystal microbalance experiments [9], whose data must, at least in some cases, embed the frictional enhancement caused by misalignment when present. Even though the time needed to diffuse-rotate a  $\sim 100$  nm-size island may be exceedingly large, the orientation angle distribution of islands will usually, under either stationary or sliding conditions, be continuous rather than delta-function like.

The general unavailability of 2D lattice orientation of incommensurate rare gas islands (as opposed to full monolayers, whose epitaxy generally differs) poses at present an obstacle to the investigation of these effects, which must nonetheless be considered as generically present and effective. The possible local misalignment of incommensurate 3D crystals in contact and its potential role in sliding friction is an even less explored, but interesting issue which remains open for future consideration.

This work was mainly supported under the ERC Advanced Grant No. 320796-MODPHYSFRICT, and partly by the Swiss National Science Foundation through a SINERGIA contract CRSII2.136287, by PRIN/COFIN Contract 2010LLKJBX 004, and by COST Action MP1303.

- 
- [1] A. Vanossi, N. Manini, M. Urbakh, S. Zapperi, and E. Tosatti, *Rev. Mod. Phys.* **85**, 529 (2013).
- [2] T. Bohlein, J. Mikhael, and C. Bechinger, *Nat. Mat.* **11**, 126 (2012).
- [3] A. Vanossi, N. Manini, and E. Tosatti, *Proc. Natl. Acad. Sci. USA* **109**, 16429 (2012).
- [4] J. Hasnain, S. Jungblut, A. Trster and C. Dellago, *Nanoscale* **6**, 10161 (2014).
- [5] A. D. Novaco and J. P. Mc Tague, *Phys. Rev. Lett.* **38**, 1286 (1977).
- [6] C. G. Shaw, S. C. Fain, and M. D. Chinn, *Phys. Rev. Lett.* **41**, 955 (1978).
- [7] T. Aruga, H. Tochiyama, and Y. Murata, *Phys. Rev. Lett.* **52**, 1794 (1984).
- [8] M. S. Tomassone, J. B. Sokoloff, A. Widom, and J. Krim, *Phys. Rev. Lett.* **79**, 4798 (1997).
- [9] J. Krim, *Adv. Phys.* **61**, 155 (2012).
- [10] M. Dienwiebel, G. S. Verhoeven, N. Pradeep, J. W. M. Frenken, J.A. Heimberg, and H.W. Zandbergen, *Phys. Rev. Lett.* **92**, 126101 (2004).
- [11] Filippov A. E., Dienwiebel M., et al., *Phys. Rev. Lett.* **100**, 046102 (2008).
- [12] S. Bleil, H. H. von Grünberg, J. Dobnikar, R. Castañeda-Priego, and C. Bechinger, *Europhys. Lett.* **73**, 450 (2006).
- [13] J. P. Mc Tague and A. D. Novaco, *Phys. Rev B* **19**, 5299 (1979).
- [14] J. Villain, *Phys. Rev. Lett.* **41**, 36 (1978).
- [15] H. Shiba, *J. Phys. Soc. Jpn* **46**, 1852 (1978).
- [16] F. Grey and J. Bohr, *Europhys. Lett.* **18**, 717 (1992).
- [17] P. San-Jose, A. Gutiérrez-Rubio, M. Sturla, and F. Guinea, *Phys. Rev. B* **90**, 075428 (2014).



# Friction Boosted by Equilibrium Misalignment of Incommensurate Two-Dimensional Colloid Monolayers– Supplemental Material

Davide Mandelli<sup>1</sup>, Andrea Vanossi<sup>2,1</sup>, Nicola Manini<sup>3,1,2</sup>, Erio Tosatti<sup>1,2,4</sup>

<sup>1</sup> *International School for Advanced Studies (SISSA), Via Bonomea 265, 34136 Trieste, Italy*

<sup>2</sup> *CNR-IOM Democritos National Simulation Center, Via Bonomea 265, 34136 Trieste, Italy*

<sup>3</sup> *Dipartimento di Fisica, Università degli Studi di Milano, Via Celoria 16, 20133 Milano, Italy*

<sup>4</sup> *International Centre for Theoretical Physics (ICTP), Strada Costiera 11, 34014 Trieste, Italy*

(Dated: March 19, 2015)

## I. MODEL DETAILS

We describe the colloidal particles as classical point-like objects interacting via a repulsive Yukawa potential

$$U_{\text{pp}}(r) = \frac{Q}{r} \exp(-r/\lambda_{\text{D}}), \quad (1)$$

where  $r$  is the interparticle distance,  $Q$  is the coupling strength, and  $\lambda_{\text{D}}$  is the Debye screening length. We restrict particle motion to two dimensions, where colloids at rest form a triangular lattice of spacing  $a_c$  in the  $(x, y)$  plane. The periodic triangular corrugation potential

$$W(\mathbf{r}) = -\frac{2}{9}U_0 \left[ \frac{3}{2} + 2 \cos \frac{2\pi x}{a_l} \cos \frac{2\pi y}{\sqrt{3}a_l} + \cos \frac{4\pi y}{\sqrt{3}a_l} \right] \quad (2)$$

$$= U_0 w(\mathbf{r})$$

has strength  $U_0$  and periodicity  $a_l$ , mimicking the experimental laser-induced optical lattice. The ratio  $\rho = a_l/a_c$  defines their relative commensurability. Here we focus on mismatched cases only, namely underdense incommensurate UI ( $\rho < 1$ ) and overdense incommensurate OI ( $\rho > 1$ ). A detailed discussion of the approximations behind this model can be found in Ref. 2.

Simulations are carried out using either constant-area periodic boundary conditions (PBC), or open boundary conditions (OBC) with a confining potential. In PBC, the purely repulsive particles are naturally confined and the total potential energy of  $N_p$  particles is

$$H = \sum_{i=1}^{N_p} \left[ W(\mathbf{r}_i) + \frac{1}{2} \sum_{j \neq i} U_{\text{pp}}(r_{ij}) \right]. \quad (3)$$

We use a triangular-lattice supercell defined by primitive vectors  $\mathbf{a}_1 = L(1, 0)$ ,  $\mathbf{a}_2 = L(0.5, \sqrt{3}/2)$  initially filled with a regularly spaced triangular monolayer of lattice constant  $a_c = 1$ , taken as our length unit. The supercell edge  $L$  and the corrugation potential wavelength are then chosen to achieve a given overall periodicity of the colloidal lattice and the periodic potential. After a number of trials, we settled on simulations using  $L = 89 a_c$  ( $N_p = 7, 891$ ) and  $\rho = 89/96 \approx 0.927$ , corresponding to the fifth approximant in the continuous fraction expansion of  $3/(1 + \sqrt{5})$ .

In OBC a large square supercell of size  $L = 500 a_c$  is partly filled by a circular island of  $N_p \simeq 30, 000$  particles,

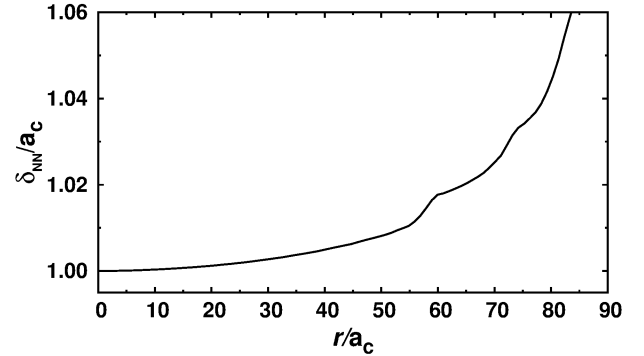


FIG. 1. Average nearest neighbor spacing as a function of the distance from the center of the model colloidal island containing  $N_p = 28, 837$  particles, optimized at rest in OBC at  $T = 0$ ,  $U_0 = 0$ , and  $\rho \simeq 0.927$ . The kinks at large radii are connected with the presence of line defects appearing in the relaxed configuration as a result of the growing inhomogeneity.

moving in the total external potential

$$V_{\text{ext}}(\mathbf{r}) = G(\mathbf{r}) [-A_G + W(\mathbf{r})], \quad (4)$$

where

$$G(\mathbf{r}) = \exp\left(-\frac{|\mathbf{r}|^2}{2\sigma_G^2}\right), \quad (5)$$

is an unnormalized confining Gaussian of large width  $\sigma_G$ . As suggested by experiment [1] both the confining amplitude  $A_G$  and the corrugation potential  $W(\mathbf{r})$  are controlled by the same Gaussian modulation. By fixing  $Q = 10^{13}$ ,  $\lambda_{\text{D}} = 0.03$ ,  $A_G = 1200$ ,  $\sigma_G = 1200$ , the Gaussian confinement and the interparticle repulsion have been balanced so as to yield an interparticle distance  $a_c \simeq 0.983$  at the island center. As shown in Fig. 1, the lattice spacing is fairly constant in the central region and increases by a few percent toward the island periphery. The total potential energy has the same expression as Eq. (3), but with  $V_{\text{ext}}(\mathbf{r}_i)$  in place of  $W(\mathbf{r}_i)$ . We carry out simulations at different lattice mismatch  $\rho = 0.927, 1.08, 0.84$  set by choosing appropriate values of  $a_l$  given the central colloidal crystal spacing  $a_c$ .

The equation of motion for the  $j$ -th particle displace-

Model Expression	Typical Value
Viscous coefficient $\eta$	$6.3 \times 10^{-8}$ kg/s
Length $a_c$	$5.7 \mu\text{m}$
Force $F = Qe^{-a_c/\lambda_D}/(\lambda_D a_c)$	20 fN
Energy $E = F a_c$	$1.1 \times 10^{-19}$ J
Velocity $V = F/\eta$	$0.3 \mu\text{m/s}$
Power $P = F^2/\eta$	$6.3 \times 10^{-21}$ W
Time $t_0 = \eta a_c/F$	18 s
Mass $m = \eta^2 a_c/F$	$1.1 \times 10^{-6}$ kg

TABLE I. Basic units for various quantities in our model and typical values mimicking the setup of Ref. 1.

ment  $\mathbf{r}_j$  is

$$m\ddot{\mathbf{r}}_j + \eta(\dot{\mathbf{r}}_j - \mathbf{v}_d) = -\nabla_{\mathbf{r}_j} \left[ \sum_{i \neq j} U_{\text{pp}}(r_{ij}) + V_{\text{ext}}(\mathbf{r}_j) \right], \quad (6)$$

where  $\mathbf{v}_d$  is the drift velocity, giving rise to a Stokes' drag force  $\mathbf{F}_d = \eta \mathbf{v}_d$ , experienced by each particle [2]. The overdamped dynamics typical of this system is achieved by adopting a sufficiently large value of the damping coefficient  $\eta$ . We use  $\eta = 28$  in all simulations. All results are expressed in terms of the basic units defined in Table I, where values are inspired by those in the experiment by Bohlein [1]. Figure 3 in the paper refers however to a different experimental setup [4] corresponding to a softer colloidal crystal at a larger lattice spacing  $a_c \simeq 6.5 \mu\text{m}$ . In that case a more appropriate value for the basic energy unit is  $E \simeq k_B T_{\text{room}} = 4.1 \times 10^{-21}$  J.

## II. SIMULATION PROTOCOLS – STATICS

In PBC the equilibrium configuration at each individual value of  $U_0$  is generated as follows. We start with a perfect colloidal crystal at  $\theta = 0^\circ$ , as sketched in Fig. 1a of the paper. A first series of zero-temperature ( $T = 0$ ) damped molecular-dynamics simulations is carried out increasing the substrate potential amplitude in steps  $\Delta U = 0.01$  from  $U_0 = 0 \rightarrow 0.5$ , relaxing the monolayer at each step until no appreciable movement of the colloids is observed. A second series of configurations is generated starting with a corrugation amplitude  $U_0 = 0.5$ , decreasing it in steps  $\Delta U = -0.05$  down to  $U_0 = 0$  and performing an annealing protocol from  $T = 1 \rightarrow 0$  at each step. The stability of each of these annealed structures is subsequently tested by further carrying out parallel  $T = 0$  relaxations varying the corrugation amplitude in steps  $\Delta U = \pm 0.01$  (both upward and downward), until  $U_0 = 0$  or  $U_0 = 0.5$  are reached. For each value of  $U_0$ , among all the configurations generated from these two procedures we eventually select the one with the lowest total energy. The resulting lowest-energy

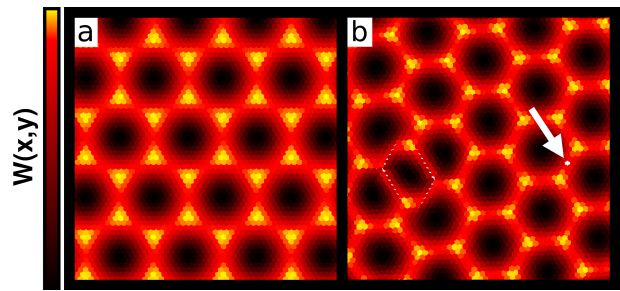


FIG. 2. A small region of the particle system optimized at rest in PBC. Particles are colored according to the local substrate potential  $W(x, y)$ . (a) Aligned ( $\theta = 0^\circ$ ) configuration obtained at  $U_0 = 0.09$ . (b) Configuration obtained at  $U_0 = 0.18$ , showing a spontaneous misalignment angle  $\theta \simeq 2.3^\circ$ , whose effect is greatly magnified in the corresponding moiré pattern, rotated by  $\psi \approx 30^\circ$  with respect to (a). An extended defect (at the left side) and a vacancy (pointed at by the arrow) appear, adapting the misaligned particle lattice to the constraint introduced by the PBC.

configuration is usually aligned for small corrugation  $U_0$ , and develops spontaneous misalignment and defects for large enough  $U_0$ , see Fig. 2.

In OBC, equilibrium configurations are generated starting from a circular island cut out of a perfect triangular crystal ( $a_c = 1$ ) and fully relaxed inside the confining potential ( $U_0 = 0$ ). The density profile resulting from the  $U_0 = 0$  relaxation is drawn in Fig. 1. We then carry out damped-dynamics simulations at  $T = 0$  increasing the corrugation  $U_0$  in steps  $\Delta U = 0.02$ . We follow the same protocol starting from islands rotated at different initial misalignment angles  $\theta_i$ , ranging between  $0^\circ \leq \theta_i \leq 30^\circ$ . From this procedure, we obtain energy curves like those in Fig. 2 of the paper, whose minima determine the optimal static configurations and equilibrium misalignment angle  $\theta_{\text{opt}}$ . Note that in this process the final orientation  $\theta_f$  of the island at the end of optimization is not identical to the initial angle  $\theta_i$ ; however, it usually remains very close. Results are then given as a function of  $\theta = \theta_i$ . All relaxed configurations with  $\theta \neq \theta_{\text{opt}}$  represent locally stable (and generally metastable) states of the system.

## III. SIMULATION PROTOCOLS – SLIDING DYNAMICS

In real sliding experiments the driving force is the viscous drag exerted on each colloid by a slow fixed-amplitude oscillatory motion of the experimental cell. The slow time scale yields long time intervals with constant drag force. Our dynamical simulations are therefore carried out by applying to each particle the same external force  $F_d = \eta v_d$ , usually along the  $x$  axis.  $F_d$  is kept constant during a finite time  $t_F$  inversely proportional to the force value  $F_d$  itself (and thus the overall

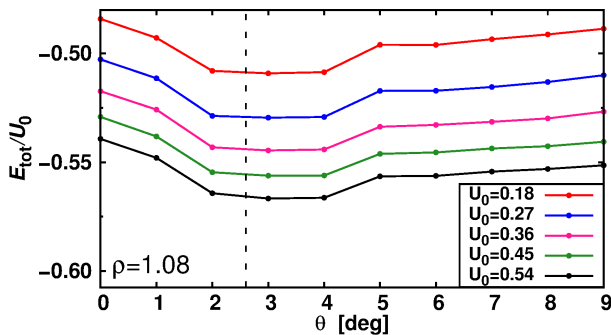


FIG. 3. Static structure optimization. Total energy per particle as a function of  $\theta$  obtained in OBC at the overdense  $\rho = 1.08$ , for different corrugations  $U_0$ . The dashed line indicates the expected value  $\theta_{\text{NM}} \simeq 2.6^\circ$  from Eq. (1) of the paper.

sliding speed). After this time, the force sign is reversed for the same time duration. The particle motion being overdamped, there are no effects of inertia. The product  $F_d t_F$  is chosen so that an isolated unconfined particle would move by a few lattice spacings  $F_d t_F / \eta \approx 2 - 3 a_c$  typically.

When we study the sliding of the monolayer in OBC, the Gaussian confining potential is kept fixed in time. Only the homogeneous central part of the island is sliding, whereas the boundary tends to remain pinned during the slow oscillatory cycle. In order to exclude undesired edge effects, we select a square central region of size  $80 \times 80 a_c^2$ , containing  $\sim 7,500$  particles. Aiming at describing steady-state sliding, we discard an initial transient of approximately 30% of the simulation time and compute averages considering particles which at  $t = 0$  were residing in this central block.

Following Ref. 2, the dissipated friction power is calculated according to Eq. (3) in the paper. Curves reported in Fig. 5 of the paper are obtained by applying this procedure to each of the misaligned static configurations produced following the protocol described earlier. We verified that due to the relatively large size of the island and the short duration of the simulations the initial angular orientation of the island is preserved during the sliding trajectory (even at finite temperature). We carried out mainly  $T = 0$  simulations integrating the equations of motions using an adaptive Runge-Kutta algorithm. When needed, thermal (Brownian) motion is simulated by adding suitable random Gaussian forces in a Langevin approach.

#### IV. OVERDENSE INCOMMENSURATE

Figure 3 displays the total energy as a function of  $\theta$  for the overdense  $\rho = 1.08$ . The theoretical NM angle is  $\theta_{\text{NM}} = 2.6^\circ$ . The minimum is found in correspondence of  $\theta_{\text{opt}} \simeq 3^\circ$ , closer to the expected value than what was

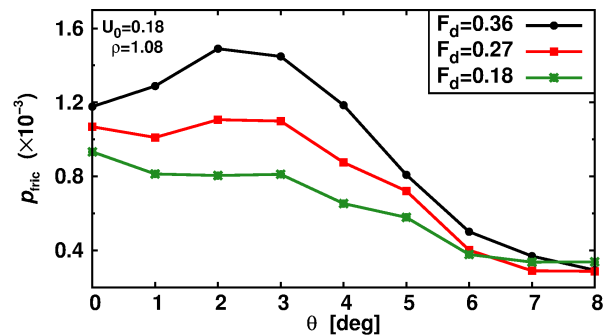


FIG. 4. Sliding dynamics in OBC. Dissipated friction power  $p_{\text{fric}}$  as a function of  $\theta$  obtained at  $\rho = 1.08$ , external forces  $F_d = 0.18, 0.27, 0.36$ , and corrugation  $U_0 = 0.18$  ( $T = 0$ ).

found in the UI regimes. In this overdense case, moving toward the periphery the average colloid spacing tends to get commensurate to the corrugation potential, favouring smaller epitaxial angles. In the OI regime the misfit stress is confined in local compressions rather than dilations. Due to the exponential form of the repulsive interaction the cost of compressions is higher, so that, at equal corrugation  $U_0$ , distortions are weaker than in the UI case. Consequently the dissipative sliding of the aligned and optimally tilted configuration is not very different and the difference in  $p_{\text{fric}}$  is reduced compared to the underdense regime. Nonetheless, far away from  $\theta_{\text{opt}}$  a significant drop of the dynamic friction is still observed, as shown in Fig. 4.

#### V. TEMPERATURE EFFECTS

The NM theory [3] assumes zero temperature. Without attempting a rigorous investigation of the problem here we anticipate, based on Eq. (1) of the paper and on finite-temperature simulations, that thermal effects do not affect the main conclusions obtained at  $T = 0$ .

Within a mean-field theory, such as a quasi-harmonic approximation, one may still use  $T = 0$  results with thermally renormalized constants. The two parameters defining  $\theta_{\text{NM}}$  are the mismatch ratio  $\rho = a_l/a_c$  and the sound velocity ratio  $\gamma = c_L/c_T$ . The mismatch ratio is under control as one can always set the desired incommensuration by fixing the average lattice spacing  $\langle a_c \rangle$ . Of course  $a_c$  will be characterized by a broader distribution at  $T \neq 0$ . Changes in the sound velocities are also irrelevant if the effects of temperature on the crystal properties act simply as a renormalization of the 2-body interaction. Under this hypothesis  $\gamma$  is expected to be weakly affected since, as it turns out, its value is mainly determined by the symmetries of the lattice [5]. Therefore in a mean-field treatment, the rotated epitaxy is expected to survive with only quantitative changes related to lattice thermal expansion.

The peak in the dynamic friction is connected with



the increased interdigitation of the monolayer within the substrate occurring at  $\theta_{\text{opt}}$ . At the optimal misalignment  $\theta_{\text{opt}}$ , solitons are enhanced, which is reflected in the larger distortions observed in the colloidal crystal (Figs. 4 and 6b of the paper), and their motion is more dissipative. At room temperature ( $k_B T_{\text{room}} \simeq 0.04$  in simulation units) we observed that such solitonic superstructures are preserved for corrugations  $U_0 > 0.1$  and dynamic friction does indeed increase near the optimal misalignment, as shown in Fig. 5.

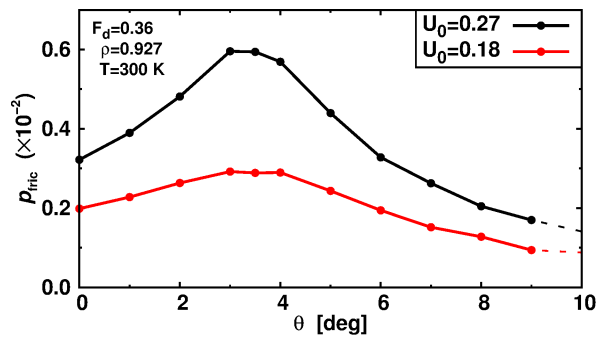


FIG. 5. The dissipated friction power  $p_{\text{fric}}$  as a function of  $\theta$  at  $T_{\text{room}}$ . Simulations have been performed in OBC, fixing  $\rho = 0.927$ , external force  $F_d = 0.36$  and corrugations  $U_0 = 0.18, 0.27$ .

- 
- [1] T. Bohlein, J. Mikhael, and C. Bechinger, Nat. Mat. **11**, 126 (2012).  
 [2] A. Vanossi, N. Manini, and E. Tosatti, Proc. Natl. Acad. Sci. USA **109**, 16429 (2012).  
 [3] A. D. Novaco and J. P. Mc Tague, Phys. Rev. Lett. **38**, 1286 (1977).  
 [4] S. Bleil, H. H. von Grünberg, J. Dobnikar, R. Castañeda-Priego, and C. Bechinger, Europhys. Lett. **73**, 450 (2006).

- [5] For any pair potential displaying a minimum and considering only nearest neighbors interactions, in a 2D triangular lattice  $c_L/c_T = \sqrt{3}$  is an exact result. Within the nearest-neighbors approximation the same result holds for the Yukawa potential of our interest for  $a_c \gg \lambda_D$ , a condition generally satisfied in actual experiments.